Heavy ion irradiation effects on the high-frequency properties of YBCO and Nb3Sn thin films

Superconductivity 13 (2025) 100149

Contents lists available at ScienceDirect

Superconductivity

journal homepage: www.elsevier.com/locate/supcon

Research article

Heavy ion irradiation effects on the high-frequency properties of YBCO and Nb_3Sn thin films

Gianluca Ghigo [a,b,*], Michela Fracasso [a,b], Roberto Gerbaldo [a,b], Daniele Torsello [a,b], Dorothea Fonnesu [c], Matteo Fretto [d], Cristian Pira [c], Natascia De Leo [d], Laura Gozzelino [a,b]

[a] Department of Applied Science and Technology, Politecnico di Torino, Torino, 10129, Italy
[b] Istituto Nazionale di Fisica Nucleare, Sezione di Torino, Torino, 10125, Italy
[c] Istituto Nazionale di Fisica Nucleare, Laboratori Nazionali di Legnaro, Legnaro, 35020, Italy
[d] Istituto Nazionale di Ricerca Metrologica, Torino, 10135, Italy

ARTICLE INFO

Keywords:
YBaCuO films
Nb3Sn films
Microwave superconductivity
Ion irradiation
Vortex pinning
Microwave coplanar resonators

ABSTRACT

High-energy heavy-ion irradiation is known to produce effective vortex pinning centers in the high-T_c cuprate superconductors, as amorphous columnar tracks. However, while the beneficial effects on pinning has been well established through dc and low-frequency characterizations, the same analysis in the high-frequency regime is far from complete. Even less investigated are the effects of heavy ion irradiation on the microwave properties of metallic low-T_c superconducting films. Here, we report on the effects of 1.15 GeV Pb irradiation on the high frequency properties of $YBa_2Cu_3O_{7-x}$ (YBCO) and Nb_3Sn thin films. The microwave analysis, performed in the range 7-8 GHz, allows obtaining the fundamental properties of both the materials, as the London penetration depth and gap values, and of the main pinning parameters, through the determination of the Campbell length by measurements in dc magnetic fields up to 4 T. GeV heavy-ion irradiation confirmed to be extremely effective for YBCO also in the high frequency regime, enhancing both the pinning constant and the depinning frequency, thus pushing the critical current density to about 30% of the depairing current density. On the other hand, the discontinuous but correlated defects produced in Nb_3Sn was found to be ineffective to enhance the pinning properties (the pinning constant in fact decreases), while the observed increment of the depinning frequency is ascribed to the reduction of the vortex viscosity, in turn due to the growth of the normal state resistivity.

1. Introduction

In order to exploit superconducting coatings for technological applications, an overall understanding of their behavior in specific conditions is needed. Recently, the demand of a full analysis of the response of superconducting films in the high-magnetic-field and high-frequency conditions stemmed from the interest to built efficient SRF axion or axion-like particle detectors, called haloscopes, to address fundamental questions concerning the physics of the dark matter [1].

Within this framework, an effort is currently made towards the full characterization of the microwave properties of superconductors when the contribution of vortices to dissipation is paramount, i.e. at fields of the order of few to several tesla. A great help in building efficient vortex dynamics models comes from studying the effects of disorder, modifying the vortex pinning landscape and thus affecting the vortex motion in a wide range of frequencies. A powerful tool to do this is ion irradiation, introducing controlled defects at the nano-scale in the material [2,3].

High-energy heavy ions are known to produce, in superconducting cuprates, amorphous tracks of insulating material that are discontinuous or continuous depending on the ion species and energy. The key parameter is the electronic stopping power, S_e, that is the amount of energy per unit length released to the target electrons via inelastic collisions. If S_e is higher than about 20 MeV/μm, columnar defects are expected in YBCO, and have been indeed observed [4,5]. The beneficial effect of these columnar defects in enhancing the vortex pinning properties of cuprates high-T_c superconductors is known from decades [6,7], but while in literature this has been extensively reported through dc and low-frequency characterizations, similar investigations for the high-frequency regime did not reach the same level of detail [8–12]. Latent tracks induced by heavy ion irradiation were also studied in the iron-based superconductors [13], and their influence on the high frequency properties was elucidated [14,15].

In more conductive metals or metal alloys, the conditions to obtain amorphization along the ion track are more difficult to achieve [16].

* Corresponding author at: Department of Applied Science and Technology, Politecnico di Torino, Torino, 10129, Italy.
E-mail address: gianluca.ghigo@polito.it (G. Ghigo).

https://doi.org/10.1016/j.supcon.2024.100149
Received 1 November 2024; Received in revised form 23 December 2024; Accepted 31 December 2024
Available online 4 January 2025

For experiments with heavy ions at the energy of a few GeV, the formation of dislocation loops is expected, clustering in the wake of the incident ion, as it was observed in the case of other metallic targets in similar conditions [17]. Understanding whether these discontinuous but correlated defects are good pinning centers or not is one of the purposes of this paper.

Specifically, in this paper we report on the effects of 1.15 GeV Pb irradiation on the high frequency properties of $YBa_2Cu_3O_{7-x}$ (YBCO) and Nb_3Sn thin films. The microwave characterization is based on the analysis of the response of coplanar-waveguide-resonators (CPWRs) patterned on the thin films under study.

The paper is organized as follows. In Section 2 we report on experimental details concerning the deposition of the films, the preparation of the devices for the microwave analysis, the high-frequency measurements and ion irradiation. In Section 3.1 the zero-field microwave characterization and the determination of basic properties of the materials, as the London penetration depth, is shown. Then, measurements in magnetic field are introduced and the way to extract the Campbell length is reported. In Section 3.2 the main pinning parameters are deduced within the Gittleman and Rosenblum approach, addressing the high-frequency vortex motion response. The ion irradiation effects are described in Section 3.3 for YBCO and Section 3.4 for Nb_3Sn. Finally, summarizing remarks and conclusions are given in Section 4.

2. Experimental details

The deposition of a set of three Nb_3Sn film samples on Al_2O_3 substrates was carried out at INFN-LNL by DC magnetron sputtering using a 4" commercial Nb_3Sn target (composition: 75% Nb, 25% Sn; purity: 99.99%). The substrates are mounted inside the UHV chamber on a holder plate, coplanar to the target and at 9 cm distance from it. The films were deposited according to the following process: the vacuum system was baked-out for 24 h at 670 °C prior to the sputtering process, which allowed reaching a base pressure of 10^{-7} mbar at 650 °C. The deposition process was carried out in argon atmosphere at $2 \cdot 10^{-2}$ mbar with the substrate temperature set at 650 °C. The power applied to the target was about 16 W (current regulated with the current fixed at 0.05 A, corresponding to an average voltage of 320 V). The deposition was carried out for 200 min, corresponding to a final film thickness of 360 nm, assessed via AFM. A post-process EDX (Energy Dispersive X-ray) analysis showed for the deposited films a Sn content of 26.2 at.%, and FESEM showed a granular structure, with an average grain size of approximately 140 nm.

Nb_3Sn CPWRs were patterned using laser lithography on a 1.5 μm thick layer of AZ3421E resist. An hardbake of 5 min at 120 °C was performed to ensure a higher resistance of the resist to the etching thus reaching the suitable selectivity for the Nb_3Sn films used (around 1 to 1). The etching process was performed with an ICP RIE from Oxford technologies using 90 sccm of SF_6 at 15 mTorr. An ICP power of 800 W and a RF table power of 40 W were chosen to optimize the balance between physical and chemical etching, with the aim of obtaining sharp and vertical sidewalls, and to avoid underetching. A laser end point detection was employed to stop the process.

Two Nb_3Sn CPWRs were considered for this study, henceforth named N#1 and N#2. For dc electrical resistivity measurements, also 100-μm-wide Hall bars were patterned.

250-nm-thick YBCO films were grown on MgO substrates via reactive thermal co-evaporation by CERACO ceramic coating GmbH (so-called "type M", with optimized critical current density) [18]. The two $YBa_2Cu_3O_{7-x}$ CPWRs considered for this study, henceforth named Y#1 and Y#2, beside Hall bars for dc resistivity measurements, were obtained by standard photolithographic process followed by wet etching.

A standard four probes technique (bias current polarity inversion and measurement averaging) was used to measure the dc resistivity vs. temperature. The critical temperature defined by means of the midpoint transition criterion is $T_c = 17.0$ K for Nb_3Sn and $T_c = 87.5$ K for YBCO,

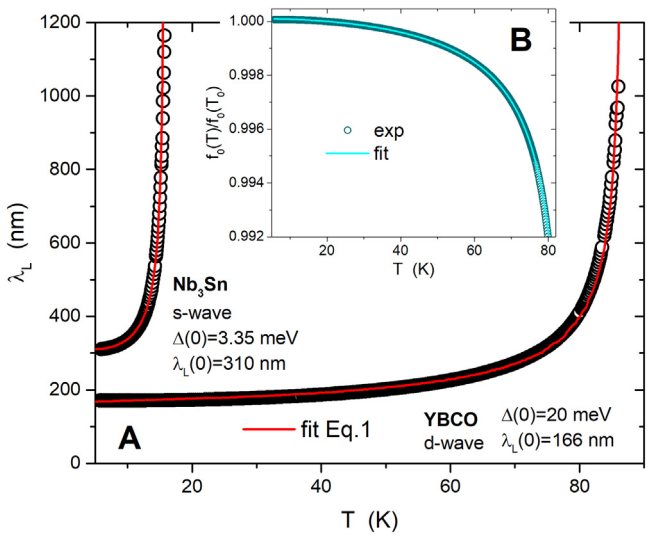

Fig. 1. (**A**) YBCO and Nb_3Sn London penetration depth vs. temperature, deduced from fitting the normalized resonance frequency (shown in **B** for the case of YBCO, see the text for details). The fitting curves shown in **A** as red lines are based on Eq. (1) (parameters reported in the graph).

the normal state resistivity at the onset of the transition is $\rho_n = 50\,\mu\Omega$cm for Nb_3Sn and $\rho_n = 65\,\mu\Omega$cm for YBCO, and the residual resistivity ratio is $RRR = \rho(295K)/\rho(17.5K) = 2.26$ for Nb_3Sn and $RRR = \rho(290K)/\rho(90K) = 3.76$ for YBCO, in accordance with literature [19,20].

The microwave characterization is based on the measurement of the resonance curves of the CPWRs, i.e. of the complex transmission coefficient (ratio of the transmitted voltage to the incident voltage) as a function of frequency, by means of a vector network analyzer. Resonance curves were measured in the range 7–8 GHz for different values of temperature and DC magnetic field [21]. In all the measurements, the external magnetic field was applied perpendicular to the film plane.

Devices were irradiated at room temperature and in vacuum with a 1.15-GeV Pb ion beam at the PIAVE-ALPI facility of the INFN Laboratori Nazionali di Legnaro, Italy, up to a fluence of $1.5 \cdot 10^{11}$ cm^{-2}. This fluence corresponds to a dose equivalent field (the magnetic field ideally needed to fill each ion track with a flux line) of $B_\phi = 3$ T. Ions were directed perpendicular to the film plane and implanted into the substrate at a depth of 40.0 μm for YBCO on MgO, and at a depth of 36.3 μm for Nb_3Sn on sapphire, as calculated by means of the Monte Carlo code SRIM [22]. No significant changes were detected after heavy-ion irradiation in the Nb_3Sn transition temperature and residual resistivity ratio, while the normal state resistivity increases by about 3%. Conversely, after irradiation, YBCO T_c, ρ_n and RRR take the values 86.5 K, 101 μΩ cm and 3.32, respectively.

In Section 3.4 we also report measurements on a Nb_3Sn CPWR irradiated with 1.5-MeV protons to a fluence of $4 \cdot 10^{16}$ cm^{-2}, for comparison. In this case, we used the AN2000 facility of the same INFN laboratories. The implantation depth of protons in sapphire is 16.7 μm and after irradiation we measured $T_c = 16.1$ K, $\rho_n = 61\,\mu\Omega$cm, and $RRR = 1.95$.

3. Results

3.1. London penetration depth and Campbell length

The analysis of the response of the CPWRs allows obtaining the absolute value of the London penetration depth, λ_L, as described in detail previously [21]. Fig. 1A shows both the cases of YBCO and Nb_3Sn, as deduced from fitting the normalized resonance frequency as a function of temperature, $f_0(T)/f_0(T_0)$, where T_0 is a fixed temperature value, selected among the lowest ones. An example of fitting curve is shown in Fig. 1B (see Ref. [21] for details, where all the expressions

needed to connect the normalized resonance frequency to the geometry of the CPWR and to the physical quantities as the penetration depth are given). In brief, the fit is made by assuming a starting parametric expression for λ_L. We chose the quite general form $\lambda_L(T) = \lambda_L(0)\left[1-(T/T_c)^\gamma\right]^{-1/2}$, which is suitable to describe different possible scenarios, depending in particular on the value of the exponent γ, that we leave as a free fitting parameter. From the fit, it resulted $\gamma = 4.0$ for Nb_3Sn, in accordance with s-wave symmetry and strong coupling [23]. For YBCO, we found $\gamma = 2.1$, in agreement with several literature reports [24–27]. This $\lambda_L(T)$ dependence is incompatible with the BCS theory, while it is consistent with the extended d-wave symmetry of the order parameter [28] or with the d-wave symmetry in the presence of significant impurity scattering [29] (see the Supplementary Material for further details).

The London penetration depth curves in turn can be analyzed to obtain other fundamental parameters such as the low-temperature value of the energy gap. To this aim, we follow the approach of Ref. [30] and consider

$$\lambda_L(T) = \lambda_L(0)\left[1+\frac{1}{\pi}\int_0^{2\pi}\int_{\Delta(\phi,T)}^{\infty}\frac{\partial f}{\partial E}\frac{E\,dE\,d\phi}{\sqrt{E^2-\Delta^2(\phi,T)}}\right]^{-1/2} \quad (1)$$

where $\Delta(\phi,T)$ is the gap function and $f = \left[1+\exp(E/k_BT)\right]^{-1}$ is the Fermi function. The angular and temperature dependencies of the gap can be factorized and approximated as $\Delta(\phi,T) = \Delta(\phi)\Delta(T) = \Delta(\phi)\tanh\left\{1.82\left[1.018\,(T_c/T-1)\right]^{0.51}\right\}$. The angular gap function is $\Delta(\phi) = \Delta_0\cos(2\phi)$ for d-wave (nodal) superconductors, while no angular dependence is considered for s-wave superconductors.

For Nb_3Sn, we chose an s-wave form for Δ and we found a reasonable agreement with data for $\Delta(0) = 3.35$ meV (Fig. 1). For YBCO, we assumed the d-wave form and got $\Delta(0) = 20$ meV. Both the values are in agreement with the literature. Also the low-temperature values of the London penetration depth are in good agreement with literature, with the quite high value for Nb_3Sn (above that expected for a clean stoichiometric Nb_3Sn) due to granularity, as recently reported in Ref. [31] for sputtered films.

This basic zero-field characterization of Nb_3Sn films gives values that are self-consistent and consistent with literature also for the combination of Sn content (26.2 at.%), critical temperature (17.0 K, midpoint), RRR (2.26), energy gap ($\Delta(0) = 3.35$ meV), and quite high normal state resistivity ($\rho_n = 50\,\mu\Omega$cm) [32–34]. The latter value is also crucial for understanding the vortex dynamics parameters and their modifications, as shown below.

In measurements in the presence of a static magnetic field, one should consider that in the mixed state a complex resistivity term, $\rho_{vm} = \rho_{vm,1} + i\rho_{vm,2}$, due to the presence and dynamics of vortices, must be added to the surface impedance, $Z_s = R_s + iX_s = \sqrt{i\mu_0\omega\left(\rho+\rho_{vm}\right)}$, that can be rewritten in terms of the Campbell length, λ_C, and conductivity, σ_C [35]. In the thin film approximation, when the Pearl length must be considered, this reads

$$\begin{aligned} Z_s &= \sqrt{-\frac{\mu_0^2\omega^2}{d^2}\left(\lambda_L^4+\lambda_C^4\right)+i\frac{\mu_0^3\omega^3\lambda_L^8}{d^4}\left(\sigma_1+\sigma_C\right)} \\ \lambda_C &= \sqrt[4]{\rho_{vm,2}d^2/\left(\mu_0\omega\right)} \\ \sigma_C &= \rho_{vm,1}d^4/\left(\mu_0^2\omega^2\lambda_L^8\right) \end{aligned} \quad (2)$$

where σ_1 is the quasiparticle conductivity and d is half the thickness of the film. We recently described in Ref. [35] the process to extract the Campbell length by comparing measurements with and without magnetic field, within the bulk limit. In the same way, but within the thin film approximation, it turns out that

$$\begin{aligned} \lambda_C(H,T) &= \sqrt[4]{\lambda(H,T)^4-\lambda_L(0,T)^4-d^2\frac{R_s(H,T)^2-R_s(0,T)^2}{\mu_0^2\omega^2}} \\ \sigma_C(H,T) &= \frac{2d^3\left[R_s(H,T)\lambda(H,T)^2-R_s(0,T)\lambda_L(0,T)^2\right]}{\mu_0^2\omega^2\lambda_L(0,T)^8} \end{aligned} \quad (3)$$

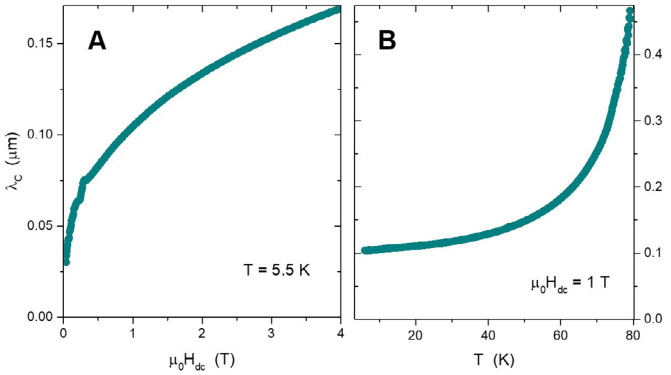

Fig. 2. Campbell length vs. magnetic field (**A**) and temperature (**B**) for the YBCO CPWR Y#1.

The resulting λ_C is shown in Fig. 2 for YBCO as a function of magnetic field (panel A) and temperature (panel B).

3.2. Pinning parameters within the GR approach

The vortex pinning parameters can be estimated by using the Gittleman and Rosenblum approach [36] (GR model, henceforth), the simplest way to model the high frequency vortex motion response that is basically described by the equation

$$\mathbf{j}\wedge\hat{\mathbf{z}}\Phi_0 - \eta\dot{\mathbf{u}} - k_p\mathbf{u} + \mathbf{F}_{th} = m\ddot{\mathbf{u}} \quad (4)$$

where $\mathbf{u}$ is the displacement, Φ_0 is the flux quantum, $\hat{\mathbf{z}}$ is the direction of the magnetic field, η is the vortex viscosity, k_p is the pinning constant, and $\mathbf{F}_{th}$ accounts for thermal fluctuation effects. Within the GR model, flux creep and vortex line bending are considered negligible,[1] and the complex vortex motion resistivity is given by

$$\rho_{vm} = \frac{\Phi_0 B}{\eta}\frac{1}{1-i\nu_p/\nu} \quad (5)$$

Here, a new parameter is introduced, the depinning frequency ν_p, a combination of previous parameters, $\nu_p = k_p/(2\pi\eta)$. It is usually considered as a sort of quality factor for high frequency applications, being the upper limit beyond which vortex motion dissipation prevails, i.e. a pinning regime is defined for $\nu < \nu_p$ and a flux-flow regime for $\nu > \nu_p$.

Through the previous equations it is possible to express the pinning parameters as a function of the Campbell length and conductivity. The expressions for the depinning frequency, the vortex viscosity and the pinning constant in the thin film limit are as follows:

$$\nu_p = \frac{\lambda_C^4 d^2}{2\pi\mu_0\sigma_C\lambda_L^8} \quad (6)$$

$$\eta = \frac{\Phi_0 B d^4}{4\pi^2\mu_0^2\nu^2\sigma_C\lambda_L^8\left[1+\lambda_C^8 d^4/\left(4\pi^2\mu_0^2\nu^2\sigma_C^2\lambda_L^{16}\right)\right]} \quad (7)$$

$$k_p = 2\pi\nu_p\eta \quad (8)$$

These parameters are reported in Fig. 3 for YBCO CPWRs, as a function of magnetic field at low temperature and as a function of temperature for two values of applied field. Data reported in the panels A, B and C show a reasonable sample-to-sample variability in the comparison between data obtained by two different CPWRs, prepared from films deposited in different runs, at years of distance. Especially at high fields, the values from the two CPWRs nicely match. From the comparison with the literature [37,38], one can conclude that the films

[1] in the case of the thin films in transverse magnetic field under study, a multi-frequency analysis (not shown here) validated these assumptions.

under study show rather high pinning constants, reflecting an optimal pinning capability. Moreover, the pinning constant allows evaluating the critical current density, J_c: an expression of J_c valid under the assumption of single vortex pinning and short range potential (effective radius of the pinning potential equal to the coherence length ξ) can be obtained by equating the Lorentz force and the pinning force, resulting in

$$J_c = k_p \xi / \Phi_0 \tag{9}$$

On the other hand, the depairing current J_{dp} can be expressed within the Ginzburg and Landau theory as [39]

$$J_{dp} = \Phi_0 / \left(3^{3/2} \pi \mu_0 \lambda_L^2 \xi\right) \tag{10}$$

Thus, both J_c and J_{dp} can be reliably estimated by means of the parameters we obtained by the microwave analysis, and assuming ξ from literature. It turns out that, for pristine YBCO at low temperatures and at the applied field of 1 T, for the two samples Y#1 and Y#2 $J_c = 4 - 6 \cdot 10^{11}\,\mathrm{A/m^2}$, corresponding to a ratio $J_c/J_{dp} = 0.11 - 0.13$, for $\xi = 1.0\,\mathrm{nm}$ [40] (further details in the Supplementary Material), i.e. J_c/J_{dp} around 10%, which is a standard value for YBCO with good but not optimized pinning landscape [41].

The pinning parameters for two Nb_3Sn CPWRs are shown in Fig. 4. Again, the sample-to-sample variability is rather narrow. The depinning frequency seems to be very high, if compared to the values reported in literature for this material in its standard compositions [42]. Indeed, Fig. 4A shows values up to about 30 GHz that are much higher than ν_p we have found in other metallic Nb-based superconductors like NbTi, by means of similar deposition technique, device design and microwave analysis [35,43]. This apparent anomaly is addressed below, by studying the effects of irradiation. As for the pinning constant (Fig. 4B), the Nb_3Sn values lay between the higher values for YBCO (Fig. 3E) and the lower ones for NbTi [35]. Pinning in Nb_3Sn is supposed to be given mainly to grain boundaries. From the pinning constant and from Eqs. (9) and (10) (and assuming $\xi = 3\,\mathrm{nm}$ [44]) it turns out that, at low temperatures and $\mu_0 H = 0.25\,\mathrm{T}$, for the two samples N#1 and N#2 $J_c = 3.6 - 5.8 \cdot 10^{10}\,\mathrm{A/m^2}$ and $J_c/J_{dp} = 0.13 - 0.17$ (further details in the Supplementary Material). This values match literature reports, where the highest pinning niobium compounds have shown critical currents of about 15% of J_{dp} [45].

3.3. Heavy ion irradiation effects on YBCO

From the above analysis, it would seem hard to increase further the pinning capability of these YBCO films. On the other hand, as stated in the Introduction, heavy-ion irradiation-induced columnar defects have proven to be among the most efficient pinning centers in YBCO. However, their effectiveness also in the high frequency range has not been investigated at the same level of details as for the dc/low frequency regime. Therefore, we irradiated the YBCO CPWR Y#2 with 1.15 GeV Pb ions, up to a dose equivalent field of B_ϕ=3 T.

Before starting the high-frequency analysis, we checked the quality of the columnar defects by measuring the irreversibility line (IL) before and after irradiation (Fig. 5). The ILs were determined from the dc resistive measurements as the temperature at which the resistivity equals 10% of the normal-state resistivity, to approximate the line above which the critical current drops to zero. In Fig. 5 it is shown that, after irradiation, the IL becomes steeper, at fields lower than B_ϕ. If at low fields a worsening was observed after irradiation (related to the enhanced charge-carrier scattering), at about $\mu_0 H_{irr} = 1.5\,\mathrm{T}$ a crossover occurs between pristine and irradiated curves, confirming the high pinning efficiency of the columnar tracks. A change of slope can be observed in the irradiated IL between $\mu_0 H_{irr} = B_\phi/2$ and $\mu_0 H_{irr} = 2B_\phi/3$. In accordance with Refs. [46,47], this kink can be the signature of a transition from a single-vortex pinning regime provided by the columnar defects to a weaker and collective pinning regime. This finding suggests that, at fields lower than the one at which the above-mentioned kink occurs, the IL can be considered a Bose-glass melting line. This line can be reported in terms of reduced temperature (temperature divided by T_c) as a function of field, $t_{BG}(B)$, and can be determined by fitting the low-field data with the relation [47]:

$$t_{BG}(B) = \frac{t_m(B) + t_{on}\gamma}{1+\gamma} \tag{11}$$

where $t_m(B)$ is the melting line of the vortex lattice in the absence of columnar defects, here obtained via a polynomial fit of IL before

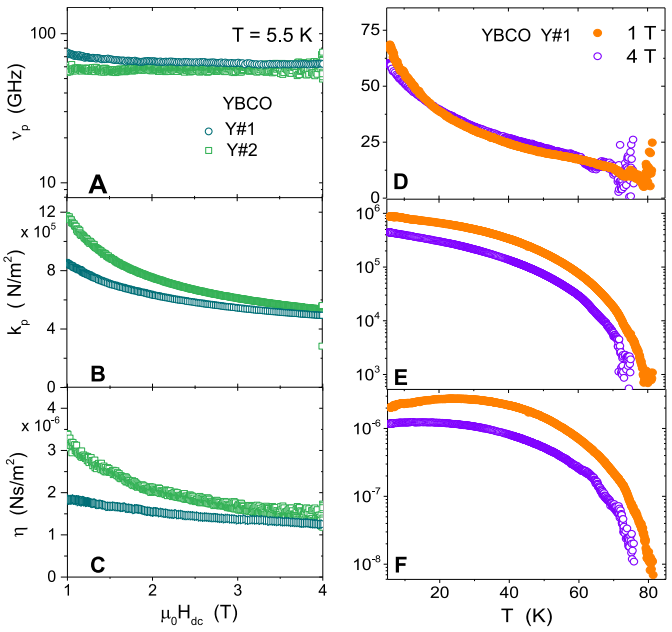

Fig. 3. Vortex pinning parameters for the YBCO CPWRs, as a function of magnetic field, for two devices Y#1 and Y#2 (left column) and as a function of temperature, for Y#1 at two magnetic fields (right column): (**A**),(**D**) depinning frequency; (**B**),(**E**) pinning constant; (**C**),(**F**) viscosity.

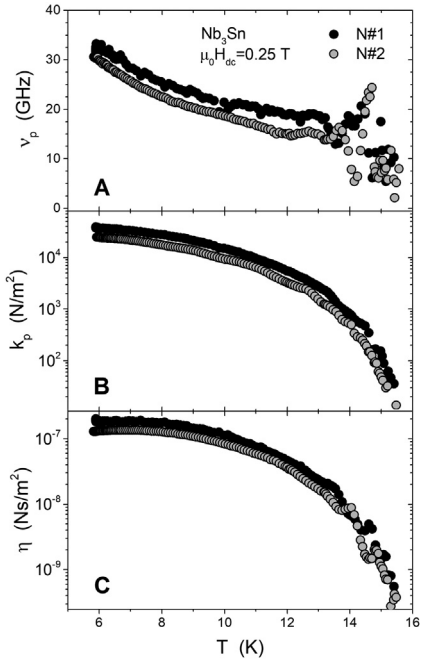

Fig. 4. Vortex pinning parameters for two Nb_3Sn CPWRs, vs. temperature: (**A**) depinning frequency; (**B**), pinning constant; (**C**) vortex viscosity.

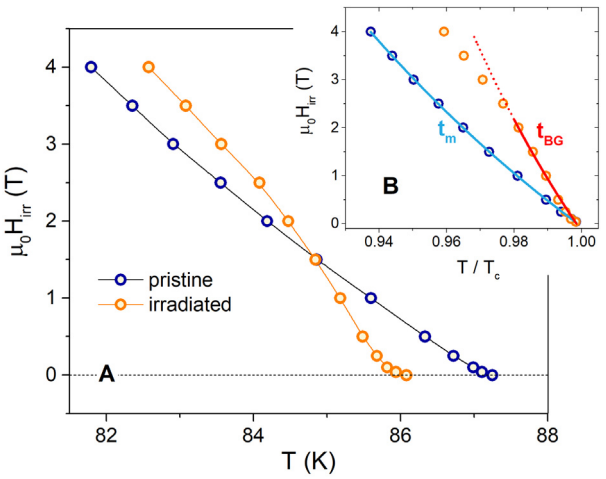

Fig. 5. (**A**) Irreversibility lines estimated from the dc resistive measurements before and after irradiation. (**B**): Same as in (**A**), as a function of the reduced temperature T/T_c. The blue curve is a polynomial fit of the before-irradiation IL, used to determine $t_m(B)$, whereas the red curve represents the best fitting curve of the low-field region of after-irradiation IL with Eq. (11).

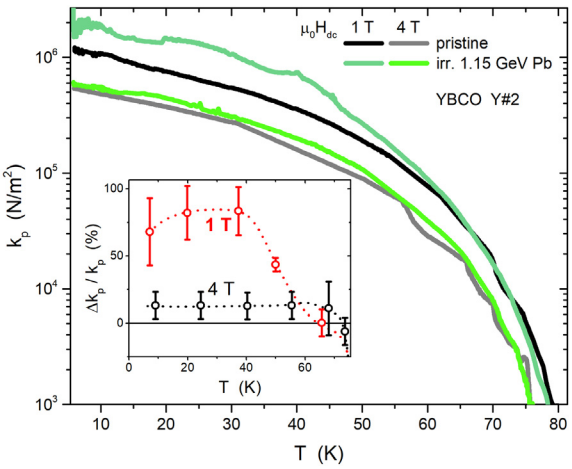

Fig. 7. Pinning constant of YBCO CPWR Y#2 vs. temperature, for two magnetic field values, before and after heavy ion irradiation. The inset shows the fractional shift of the pinning constant after irradiation (red and black dotted curves; some points are reported to show the errors).

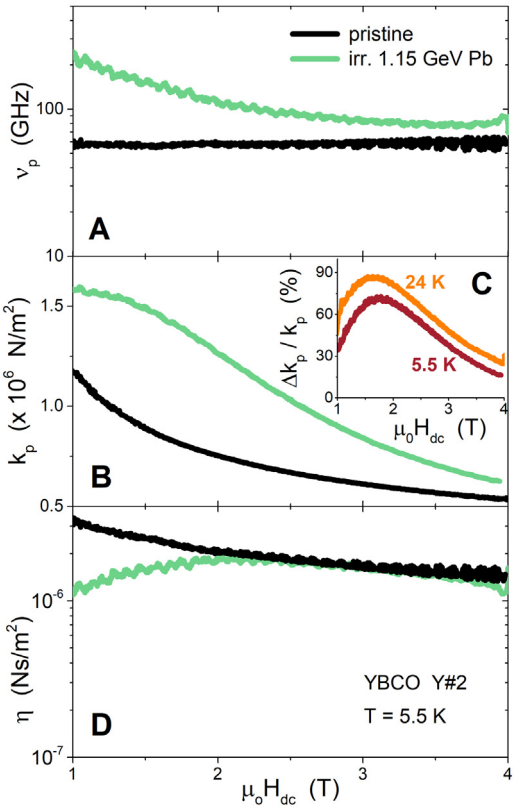

Fig. 6. Pinning parameters of YBCO Y#2 vs. magnetic field, before (black) and after (green) heavy ion irradiation: (**A**) depinning frequency; (**B**) pinning constant; (**C**) pinning constant fractional shift after irradiation, at two temperatures; (**D**) vortex viscosity.

irradiation (see Fig. 5B), and $t_{on} = T_{on}/T_c$ and γ are the fitting parameters. T_{on} represents the maximum temperature at which the columns are effective pinning centers (that in principle could be lower than T_c) and γ can be expressed as $\gamma = b_0^2/\left(16\,a\,\xi_{ab}(0)G^{1/2}\right)$, where in turn b_0 is the confining diameter of the columnar defects, a is the average distance between the columns ($a = \sqrt{\Phi_0/B_\phi} = 25.9$ nm for $B_\phi = 3$ T), $\xi_{ab}(0) = 1.2$ nm is the coherence length, and $Gi = 0.004$ is the Ginzburg number. The best fit, shown in Fig. 5B, was obtained for $t_{on} = 0.997 \pm 0.001$ and $\gamma = 1.06 \pm 0.06$. Noteworthy, this value of γ gives $b_0 = 5.8$ nm, i.e. a value totally consistent with the diameter of the irradiation-induced columnar defects in YBCO [48]. In conclusion, this dc analysis confirms the formation of highly-effective columnar pinning centers in the YBCO films under study, after 1.15-GeV Pb irradiation.

Then, the modifications produced on the pinning parameters at low temperatures were investigated by the microwave analysis, and are reported in Fig. 6, as a function of the magnetic field. One can notice a clear improvement of the pinning constant (panel B). In the graph C it is shown that this improvement is not monotonic, and that the fractional shift of k_p displays a broad maximum at a field between $B_\phi/2$ and $2B_\phi/3$. This means that the optimal matching between the vortex lattice and the columnar defect array occurs at the same fields where the dc analysis showed the kink in the irradiated IL. The panel A shows an increased depinning frequency, that is due both to the improvement in the pinning capability and to the decrease of the viscosity at low fields (panel D), in turn due to the increase of the normal state resistivity.

The increase of the pinning constant for the irradiated CPWR was also investigated as a function of temperature. It is shown in Fig. 7 for two values of the applied magnetic field. The fractional increment of k_p is reported in the inset, showing that the highest enhancement is at low temperatures and for fields lower than B_ϕ, that it is still present but lower for fields higher than B_ϕ, and that it is absent at temperatures above about 60 K.

As for the current densities, both J_c and J_{dp} are affected by irradiation: the former is expected to increase due to enhanced pinning, the latter to decrease due to enhanced charge-carrier scattering (that in the case of high-energy heavy-ion irradiation is mainly provided by small defects produced by secondary recoils around the columnar tracks). At low temperatures and at the applied field of 1 T, the irradiated Y#2 shows $J_c \approx 8 \cdot 10^{11}$ A/m^2, higher than the value before irradiation. Also the J_c/J_{dp} ratio is increased. It has been reported that this ratio cannot reach values much above 30% [6,45], in the ideal case of columnar defects when thermal relaxation can be neglected. Indeed, we obtained $J_c/J_{dp} = 0.26$ (for $\xi = 1.0$ nm), therefore our result probably represents the experimental achievement of the optimal vortex pinning state in YBCO.

3.4. Heavy ion irradiation effects on Nb_3Sn

As stated above, the depinning frequency for the Nb_3Sn CPWR results to be very high. This apparent anomaly can be due either to

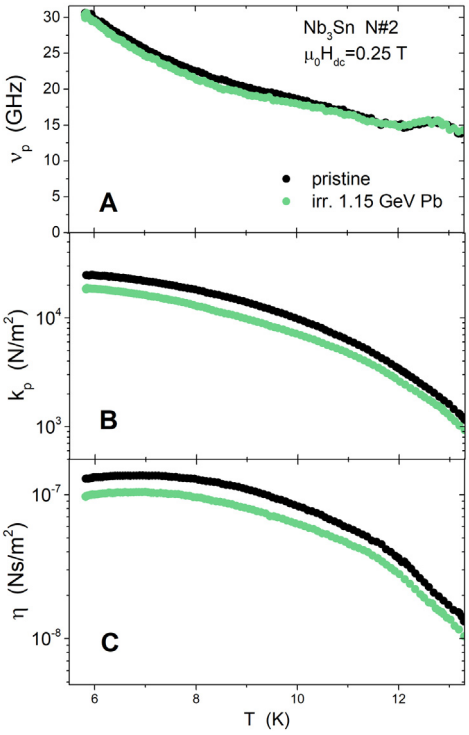

Fig. 8. (**A**) depinning frequency, (**B**) pinning constant, (**C**) vortex viscosity, for Nb_3Sn before (black) and after (green) heavy ion irradiation. The curves are shown as a function of temperature for an applied magnetic field of 0.25 T.

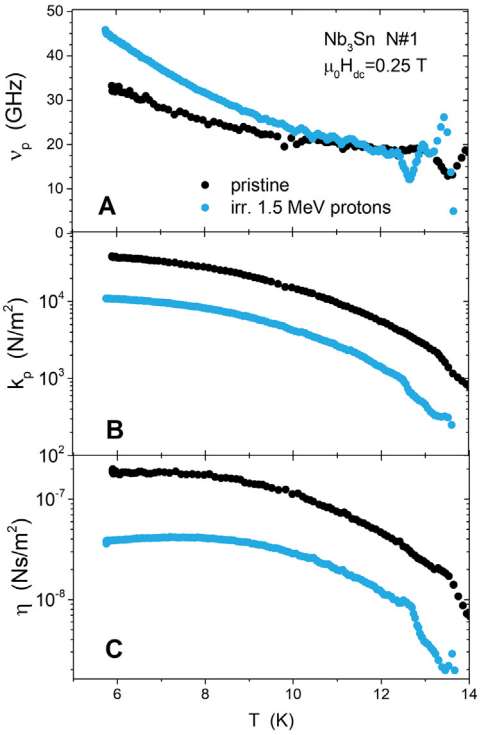

Fig. 9. Effects of proton irradiation on the Nb_3Sn film (black: pristine, blue: irradiated): (**A**) depinning frequency, (**B**) pinning constant, (**C**) vortex viscosity vs. temperature for an applied magnetic field of 0.25 T.

extremely good pinning or to low vortex viscosity (see Eq. (8)), in turn due to high normal-state resistivity (for the ν_p dependence on the mean-free-path see also Ref. [49]).

To investigate which is the actual reason for the ν_p anomaly, we changed the pinning landscape by heavy ion irradiation. In fact, in this case the irradiation experiment had a twofold aim. Beside investigating the origin of the ν_p anomaly, we wanted to check the efficiency of the defects produced by GeV heavy ions in the metallic Nb_3Sn. As discussed in the Introduction, we expect in this case clusters of dislocation loops along the ion path, rather then amorphous tracks as in YBCO. Therefore the question arises whether these linearly correlated structural defects behave like columnar defects in YBCO, in terms of pinning efficiency.

Fig. 8 shows that 1.15 GeV Pb irradiation is not able to enhance pinning in Nb_3Sn, on the contrary k_p slightly decreases (panel B). Also the viscosity decreases, of a similar amount (panel C), thus giving a practically unchanged depinning frequency (panel A). In other words, in this case the increase of normal state resistivity after irradiation "masked" the worsening of the pinning capability, keeping ν_p to an high value.

To understand whether this mechanism can be pushed further, we tried to increase much more the charge carrier scattering, by introducing a high density of small defects. This was done by 1.5-MeV proton irradiation up to a dose of $4 \cdot 10^{16}\,\mathrm{cm}^{-2}$. Results are shown in Fig. 9. The irradiation-induced defects are not as effective as pinning centers and probably irradiation negatively affects the main pinning mechanism active in the pristine material, i.e. the grain boundary network. However, the vortex viscosity reduction is much stronger, thus pushing ν_p to even higher values. This result shed more light into the issue of the ν_p anomaly: its high values in the pristine material could be ascribed to the fact that, due to Sn excess, the normal state resistivity of these films is quite high. The issue deserving further investigation is the fact that quantitatively η and ρ_n modifications after irradiation do not seem to fit the Bardeen-Stephen formula $\eta = \Phi_0 B_{c2}/\rho_n$.

4. Summarizing remarks and conclusions

A careful high-frequency analysis of two key materials, YBCO and Nb_3Sn, promising as coatings for a number of applications, was carried out by means of a technique based on the use of coplanar waveguide resonators. Zero-field rf measurements allowed characterizing fundamental properties of the materials, such as the London penetration depth and the energy gap. Data for both the materials showed internal self-consistency and consistency with literature, and thus allowed fixing some parameters useful for the following analysis. Rf measurements were then performed with DC magnetic fields up to 4 T, to investigate the vortex dynamics contribution to dissipation and in general to the response of the devices. The Campbell length and conductivity can be estimated and used to express the main pinning parameters, within the Gittleman and Rosenblum approach to model the high frequency vortex motion response. Finally, the CPWRs were irradiated with 1.15 GeV Pb ions and the effects of the resulting defects were investigated by repeating the whole characterization on the same devices.

Amorphous columnar defects induced in YBCO by GeV heavy-ion irradiation confirmed to be extremely effective in the high frequency regime. They enhance both the pinning constant (reaching about $2 \cdot 10^6\,\mathrm{N/m}^2$ at 5 K and 1 T) and the depinning frequency (overcoming 100 GHz), thus pushing the critical current density to about 30% of the depairing current density. This result is among the best ones reported in literature for columnar defects in YBCO. Beside testifying the achievement of the optimal pinning condition, it confirms the reliability of microwave techniques for the investigation of general properties of superconductors.

On the other hand, the same Pb ions did not enhance vortex pinning in Nb_3Sn films, in agreement with the fact that this kind of irradiation in metallic films generates clusters of dislocation loops along the ion path rather than amorphous and continuous tracks. It turns out that these discontinuous but correlated defects are ineffective to enhance the vortex pinning properties. In fact, the pinning constant decreased

after irradiation. We observed an increment of the depinning frequency, but this is ascribed to the reduction of the vortex viscosity rather than to a pinning effect.

CRediT authorship contribution statement

Gianluca Ghigo: Writing – original draft, Supervision, Methodology, Investigation, Conceptualization. **Michela Fracasso:** Writing – review & editing, Data curation. **Roberto Gerbaldo:** Investigation, Data curation. **Daniele Torsello:** Writing – review & editing, Investigation. **Dorothea Fonnesu:** Data curation. **Matteo Fretto:** Writing – review & editing, Investigation. **Cristian Pira:** Writing – review & editing, Validation, Resources. **Natascia De Leo:** Writing – review & editing, Investigation. **Laura Gozzelino:** Writing – review & editing, Supervision, Investigation.

Declaration of competing interest

The authors declare that they have no known competing financial interests or personal relationships that could have appeared to influence the work reported in this paper.

Acknowledgments

This work received partial support from INFN-CSN5 under the S.A.M.A.R.A. experiment. D.T. acknowledges that his contribution was carried out within the Ministerial Decree no. 1062/2021 and received funding from the FSE REACT-EU PON Ricerca e Innovazione 2014–2020. This manuscript reflects only the authors' views and opinions, neither the European Union nor the European Commission can be considered responsible for them.

Appendix A. Supplementary data

Supplementary material related to this article can be found online at https://doi.org/10.1016/j.supcon.2024.100149.

References

[1] Semertzidis YK, Youn S. Axion dark matter: How to see it? Sci Adv 2022;8(8):eabm9928. http://dx.doi.org/10.1126/sciadv.abm9928.
[2] Zhu Y, Cai ZX, Budhani RC, Suenaga M, Welch DO. Structures and effects of radiation damage in cuprate superconductors irradiated with several-hundred-MeV heavy ions. Phys Rev B 1993;48:6436–50. http://dx.doi.org/10.1103/PhysRevB.48.6436.
[3] Kirk M. Structure and flux pinning properties of irradiation defects in $YBa_2Cu_3O_{7-x}$. Cryogenics 1993;33(3):235–42.
[4] Hardy V, Provost J, Groult D, Simon C, Hervieu M, Raveau B. Columnar defects induced by high energy heavy ions in HTSC. Their effect on irreversibility line and pinning properties. J Alloys Compd 1993;195:395–402. http://dx.doi.org/10.1016/0925-8388(93)90764-E.
[5] Lang M, Djurabekova F, Medvedev N, Toulemonde M, Trautmann C. Fundamental phenomena and applications of swift heavy ion irradiations. In: Konings RJ, Stoller RE, editors. Comprehensive nuclear materials (second edition). second ed. Oxford: Elsevier; 2020, p. 485–516. http://dx.doi.org/10.1016/B978-0-12-803581-8.11644-3.
[6] Civale L, Marwick AD, Worthington TK, Kirk MA, Thompson JR, Krusin-Elbaum L, Sun Y, Clem JR, Holtzberg F. Vortex confinement by columnar defects in $YBa_2Cu_3O_7$ crystals: Enhanced pinning at high fields and temperatures. Phys Rev Lett 1991;67:648–51. http://dx.doi.org/10.1103/PhysRevLett.67.648.
[7] Civale L. Vortex pinning and creep in high-temperature superconductors with columnar defects. Supercond Sci Technol 1997;10(7A):A11.
[8] Lofland SE, Bhagat SM, Rajeswari M, Venkatesan T, Kanjilal D, Senapati L, Mehta GK. Microwave observation of the vortex locked-in state in $YBa_2Cu_3O_7$ thin films with columnar defects. Phys Rev B 1995;51:8489–93. http://dx.doi.org/10.1103/PhysRevB.51.8489.
[9] Banerjee T, Kanjilal D, Pinto R. Peak effect and its evolution with defect structure in $YBa_2Cu_3O_{7-\delta}$ thin films at microwave frequencies. Phys Rev B 2002;65:174521. http://dx.doi.org/10.1103/PhysRevB.65.174521.
[10] Ghigo G, Laviano F, Gerbaldo R, Gozzelino L. Tuning the response of YBCO microwave resonators by heavy-ion patterned micro-channels. Supercond Sci Technol 2012;25(11):115007. http://dx.doi.org/10.1088/0953-2048/25/11/115007.
[11] Ghigo G, Botta D, Chiodoni A, Gerbaldo R, Gozzelino L, Laviano F, Minetti B, Mezzetti E, Andreone D. Microwave dissipation in YBCO coplanar resonators with uniform and non-uniform columnar defect distribution. Supercond Sci Technol 2004;17(8):977. http://dx.doi.org/10.1088/0953-2048/17/8/004.
[12] Ghigo G, Andreone D, Botta D, Chiodoni A, Gerbaldo R, Gozzelino L, Laviano F, Minetti B, Mezzetti E. Non-uniform columnar defect implantation in YBCO coplanar resonators for the control of vortex-induced microwave dissipation and nonlinearity. Supercond Sci Technol 2004;18(1):193. http://dx.doi.org/10.1088/0953-2048/18/1/030.
[13] Massee F, Sprau PO, Wang Y-L, Davis JCS, Ghigo G, Gu GD, Kwok W-K. Imaging atomic-scale effects of high-energy ion irradiation on superconductivity and vortex pinning in Fe(Se,Te). Sci Adv 2015;1(4):e1500033. http://dx.doi.org/10.1126/sciadv.1500033.
[14] Ghigo G, Ummarino G, Gozzelino L, Gerbaldo R, Laviano F, Torsello D, Tamegai T. Effects of disorder induced by heavy-ion irradiation on $(Ba_{1-x}K_x)Fe_2As_2$ single crystals, within the three-band Eliashberg s± wave model. Sci Rep 2017;7(1):13029.
[15] Ghigo G, Torsello D, Gerbaldo R, Gozzelino L, Laviano F, Tamegai T. Effects of heavy-ion irradiation on the microwave surface impedance of $(Ba_{1-x}K_x)Fe_2As_2$ single crystals. Supercond Sci Technol 2018;31(3):034006. http://dx.doi.org/10.1088/1361-6668/aaa858.
[16] Barbu A, Dunlop A, Lesueur D, Averback R. Latent tracks do exist in metallic materials. Europhys Lett 1991;15(1):37.
[17] Studer F, Hervieu M, Costantini J-M, Toulemonde M. High resolution electron microscopy of tracks in solids. Nucl Instrum Methods Phys Res B 1997;122(3):449–57.
[18] Utz B, Semerad R, Bauer M, Prusseit W, Berberich P, Kinder H. Deposition of YBCO and NBCO films on areas of 9 inches in diameter. IEEE Trans Appl Supercond 1997;7(2):1272–7. http://dx.doi.org/10.1109/77.620749.
[19] Arpaia R, Golubev D, Baghdadi R, Ciancio R, Dražić G, Orgiani P, Montemurro D, Bauch T, Lombardi F. Transport properties of ultrathin $YBa_2Cu_3O_{7-\delta}$ nanowires: A route to single-photon detection. Phys Rev B 2017;96(6):064525.
[20] Kuriki S, Takahashi K-i, Kawaguchi Y, Matsuda M, Otowa T. High critical current density YBCO films and fabrication of dc-SQUIDs. Supercond Sci Technol 2002;15(12):1693.
[21] Ghigo G, Torsello D. Microwave Analysis of Unconventional Superconductors with Coplanar-Resonator Techniques. Springer; 2022.
[22] Ziegler JF, Ziegler M, Biersack J. SRIM – the stopping and range of ions in matter (2010). Nucl Instrum Methods Phys Res B 2010;268(11):1818–23. http://dx.doi.org/10.1016/j.nimb.2010.02.091, 19th International Conference on Ion Beam Analysis.
[23] Linden DS, Orlando TP, Lyons WG. Modified two-fluid model for superconductor surface impedance calculation. IEEE Trans Appl Supercond 1994;4(3):136–42.
[24] Bonn DA, Liang R, Riseman TM, Baar DJ, Morgan DC, Zhang K, Dosanjh P, Duty TL, MacFarlane A, Morris GD, Brewer JH, Hardy WN, Kallin C, Berlinsky AJ. Microwave determination of the quasiparticle scattering time in $YBa_2Cu_3O_{6.95}$. Phys Rev B 1993;47:11314–28. http://dx.doi.org/10.1103/PhysRevB.47.11314.
[25] Brorson SD, Buhleier R, White JO, Trofimov IE, Habermeier H-U, Kuhl J. Kinetic inductance and penetration depth of thin superconducting films measured by THz-pulse spectroscopy. Phys Rev B 1994;49:6185–7. http://dx.doi.org/10.1103/PhysRevB.49.6185.
[26] Vendik O, Vendik I, Kaparkov D. Empirical model of the microwave properties of high-temperature superconductors. IEEE Trans Microw Theory Tech 1998;46(5):469–78. http://dx.doi.org/10.1109/22.668643.
[27] Pond JM, Carroll KR, Horwitz JS, Chrisey DB, Osofsky MS, Cestone VC. Penetration depth and microwave loss measurements with a $YBa_2Cu_3O_7 - \delta/LaAlO_3/YBa_2Cu_3O_7 - \delta$ trilayer transmission line. Appl Phys Lett 1991;59(23):3033–5. http://dx.doi.org/10.1063/1.105784.
[28] Prozorov R. Superfluid density in a superconductor with an extended d-wave gap. Supercond Sci Technol 2008;21(8):082003.
[29] Arberg P, Mansor M, Carbotte J. Penetration depth for a 2D D-wave superconductor. Solid State Commun 1993;86(10):671–3. http://dx.doi.org/10.1016/0038-1098(93)90837-D.
[30] Chandrasekhar BS, Einzel D. The superconducting penetration depth from the semiclassical model. Ann Phys. 1993;505(6):535–46.
[31] Makita J, Sundahl C, Ciovati G, Eom CB, Gurevich A. Nonlinear Meissner effect in Nb_3Sn coplanar resonators. Phys Rev Res 2022;4:013156. http://dx.doi.org/10.1103/PhysRevResearch.4.013156.
[32] Moore DF, Zubeck RB, Rowell JM, Beasley MR. Energy gaps of the A-15 superconductors Nb_3Sn, V_3Si, and Nb_3Ge measured by tunneling. Phys Rev B 1979;20:2721–38. http://dx.doi.org/10.1103/PhysRevB.20.2721.
[33] Orlando TP, McNiff EJ, Foner S, Beasley MR. Critical fields, Pauli paramagnetic limiting, and material parameters of Nb_3Sn and V_3Si. Phys Rev B 1979;19:4545–61. http://dx.doi.org/10.1103/PhysRevB.19.4545.
[34] Sayeed MN, Pudasaini U, Reece CE, Eremeev GV, Elsayed-Ali HE. Properties of Nb_3Sn films fabricated by magnetron sputtering from a single target. Appl Surf Sci 2021;541:148528. http://dx.doi.org/10.1016/j.apsusc.2020.148528.
[35] Ghigo G, Torsello D, Gozzelino L, Fracasso M, Bartoli M, Pira C, Ford D, Marconato G, Fretto M, De Carlo I, et al. Vortex dynamics in NbTi films at high frequency and high DC magnetic fields. Sci Rep 2023;13(1):9315.

[36] Gittleman JI, Rosenblum B. Radio-frequency resistance in the mixed state for subcritical currents. Phys Rev Lett 1966;16:734–6. http://dx.doi.org/10.1103/PhysRevLett.16.734.

[37] Golosovsky M, Tsindlekht M, Davidov D. High-frequency vortex dynamics in $YBa_2Cu_3O_7$. Supercond Sci Technol 1996;9(1):1.

[38] Bartolomé E, Alcalà J, Vallés F, Puig T, Obradors X, Pompeo N, Alimenti A, Torokhtii K, Rizzo F, Augieri A, et al. Vortex pinning properties at dc and microwave frequencies of $YBa_2Cu_3O_{7-x}$ films with nanorods and nanoparticles. Supercond Sci Technol 2020;33(7):074006.

[39] Tinkham M. Introduction to superconductivity, vol. 1. Courier Corporation; 2004.

[40] Ando Y, Segawa K. Magnetoresistance of untwinned $YBa_2Cu_3O_y$ single crystals in a wide range of doping: Anomalous hole-doping dependence of the coherence length. Phys Rev Lett 2002;88:167005. http://dx.doi.org/10.1103/PhysRevLett.88.167005.

[41] Miura M, Tsuchiya G, Harada T, Sakuma K, Kurokawa H, Sekiya N, Kato Y, Yoshida R, Kato T, Nakaoka K, et al. Thermodynamic approach for enhancing superconducting critical current performance. NPG Asia Mater 2022;14(1):85.

[42] Alimenti A, Pompeo N, Torokhtii K, Spina T, Flükiger R, Muzzi L, Silva E. Microwave measurements of the high magnetic field vortex motion pinning parameters in Nb_3Sn. Supercond Sci Technol 2020;34(1):014003.

[43] Ghigo G, Fracasso M, Gerbaldo R, Torsello D, Pira C, Marconato G, Fretto M, De Leo N, Gozzelino L. Vortex-induced nonlinearity and the effects of ion irradiation on the high-frequency response of NbTi films. Results Phys 2024;57:107437. http://dx.doi.org/10.1016/j.rinp.2024.107437.

[44] Godeke A. Nb_3Sn for radio frequency cavities. Tech. Rep., Lawrence Berkeley National Lab.(LBNL), Berkeley, CA (United States); 2006.

[45] Arcos DH, Kunchur MN. Suppressed flux motion in magnesium diboride films. Phys Rev B 2005;71:184516. http://dx.doi.org/10.1103/PhysRevB.71.184516.

[46] Krusin-Elbaum L, Civale L, Blatter G, Marwick A, Holtzberg F, Feild C. Bose-glass melting in YBaCuO crystals with correlated disorder. Phys Rev Lett 1994;72(12):1914.

[47] Mezzetti E, Gerbaldo R, Ghigo G, Gozzelino L, Minetti B, Camerlingo C, Monaco A, Cuttone G, Rovelli A. Control of the critical current density in $YBa_2Cu_3O_7 - \delta$ films by means of intergrain and intragrain correlated defects. Phys Rev B 1999;60(10):7623.

[48] Laviano F, Botta D, Chiodoni A, Gerbaldo R, Ghigo G, Gozzelino L, Mezzetti E. Evidence of vortex curvature and anisotropic pinning in superconducting films by quantitative magneto-optics. Phys Rev B 2003;68(1):014507.

[49] Checchin M, Martinello M, Grassellino A, Romanenko A, Zasadzinski J. Electron mean free path dependence of the vortex surface impedance. Supercond Sci Technol 2017;30(3):034003.